Detailed Modeling of Low-Temperature Propane Oxidation: 1. The Role of the Propyl + O-2 Reaction

ARTICLE *in* THE JOURNAL OF PHYSICAL CHEMISTRY A · JUNE 2010

Impact Factor: 2.69 · DOI: 10.1021/jp1017218 · Source: PubMed

3 AUTHORS, INCLUDING:

Lam Huynh
Vietnam National University, Ho Chi Minh …
40 PUBLICATIONS **585** CITATIONS

SEE PROFILE

Anthony M Dean
Colorado School of Mines
158 PUBLICATIONS **3,943** CITATIONS

SEE PROFILE

Detailed Modeling of Low-Temperature Propane Oxidation: 1. The Role of the Propyl + O_2 Reaction

Lam K. Huynh, Hans-Heinrich Carstensen, and Anthony M. Dean*

Chemical Engineering Department, Colorado School of Mines, Golden, Colorado 80401

Received: February 25, 2010; Revised Manuscript Received: May 4, 2010

Accurate description of reactions between propyl radicals and molecular oxygen is an essential prerequisite for modeling of low-temperature propane oxidation because their multiple reaction pathways either accelerate the oxidation process via chain branching or inhibit it by forming relatively stable products. The CBS-QB3 level of theory was used to construct potential energy surfaces for *n*-C_3H_7 + O_2 and *i*-C_3H_7 + O_2. High-pressure rate constants were calculated using transition state theory with corrections for tunneling and hindered rotations. These results were used to derive pressure- and temperature-dependent rate constants for the various channels of these reactions under the framework of the Quantum Rice—Ramsperger—Kassel (QRRK) and the modified strong collision (MSC) theories. This procedure resulted in a thermodynamically consistent C_3H_7 + O_2 submechanism, which was either used directly or as part of a larger extended detailed kinetic mechanism to predict the loss of propyl and the product yields of propylene and HO_2 over a wide range of temperatures, pressures, and residence times. The overall good agreement between predicted and experimental data suggests that this reaction subset is reliable and should be able to properly account for the reactions of propyl radicals with O_2 in propane oxidation. It is also demonstrated that for most conditions of practical interest only a small subset of reactions (e.g., isomerization, concerted elimination of HO_2, and stabilization) controls the oxidation kinetics, which makes it possible to considerably simplify the mechanism. Moreover, we observed strong similarities in the rate coefficients within each reaction class, suggesting the potential for development of relatively simple rate constant estimation rules that could be applied to analogous reactions involving hydrocarbon radicals that are too large to allow accurate detailed electronic structure calculations.

I. Introduction

Given its significant importance in combustion ignition systems, low-temperature oxidation chemistry has been the subject of intense studies for many years.[1] As a result, detailed kinetic models are available to describe the ignition behavior of a wide range of hydrocarbon fuels with good accuracy,[2−4] and current efforts focus on extending those mechanisms to surrogate mixtures for gasoline,[5] diesel,[6] and jet fuels.[7] One common feature of the most widely used kinetic models is that they are developed in a systematic way based on well-defined reaction classes[8] and rate estimation methods. The modular concept helps to make these mechanisms relatively easy to maintain, transparent, and extendable.

A key reaction in the low-temperature oxidation of alkanes is the addition of alkyl radicals to molecular oxygen. This reaction produces either stabilized alkyl peroxy radicals and their hydroperoxy alkyl isomers, or bimolecular products such as hydroperoxy radicals together with olefins or cyclic alkanes, or hydroxyl radicals with aldehydes, ketones, or cyclic ethers. Shown in Scheme 1 are important channels for this reaction, where "R" and "Q" denote C_nH_{2n+1} and C_nH_{2n} groups, respectively; "M" represents a collider; "•" symbolizes a radical site; and "*" designates an energized/activated species.

Since the C−O bond is rather weak, alkyl peroxy radicals (ROO•) can easily redissociate at elevated temperatures. The reversibility of the R + O_2 reaction is considered the main cause of the observed negative temperature coefficient region seen in ignition experiments.[1] Note the multiple reaction pathways for ROO• and its isomer Q•OOH. The rate constants for the various pathways depend on both temperature and pressure, making the kinetic analysis of this system quite complicated. These various reaction channels might either accelerate the overall reaction via chain branching or inhibit it by producing relatively inert species such as HO_2. Given the importance of this reaction class, a kinetic description of it is found in every detailed kinetic mechanism describing ignition chemistry, even though the level of detail may vary.

SCHEME 1

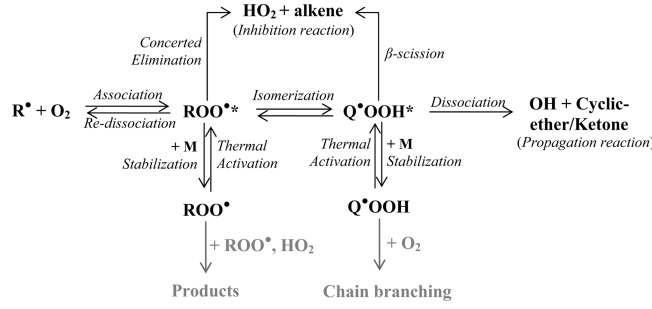

Our understanding of the elementary steps of the R + O_2 reaction changed profoundly when almost a decade ago Rienstra-Kirakofe et al.[9] discovered for the ethyl + O_2 reaction a new reaction pathway: the concerted HO_2 elimination reaction. Incorporation of this reaction channel into the ethyl + O_2 submechanism[10,11] showed that it was able to predict experimental results of several studies[12−14] that could not satisfactorily be explained previously.[15] Similar conclusions can be drawn

* To whom correspondence should be addressed. E-mail: amdean@mines.edu.

10.1021/jp1017218
Published on Web 05/28/2010

for higher alkyl + O_2 reactions.[16] Therefore, it has been recognized that this reaction channel needs to be incorporated into low-temperature oxidation mechanisms.[3] This in turn requires a rate estimation rule be developed for this channel. Additionally, since it competes with existing previously considered reaction pathways, rate constants for these reactions might need to be modified as well. One way to obtain such rate estimation rules is to investigate the R + O_2 reaction for small alkyl radicals theoretically with high-level electronic structure calculations. This is one of the motivations of the current study. Since the ethyl + O_2 reaction has already been analyzed, we focus here on the reaction of propyl radicals with molecular oxygen.

The propyl + O_2 reaction is the smallest realistic prototype of the alkyl + O_2 reaction class, because it contains most of the essential reaction pathways that play a role in larger systems. The short alkyl chains of methyl and ethyl radicals result in high barriers for isomerization reactions of the alkyl peroxy radicals; such isomerizations are much more important for radicals with longer alkyl chains. Hence, methyl and ethyl reactions with O_2 are special cases, which, although interesting in their own right, are not suitable to create a general and complete understanding of the alkyl + O_2 chemistry. Because of their role as a model system, the reactions of propyl radicals with oxygen have been subject of numerous experimental[17−29] and theoretical[29−34] studies. For example, Taatjes and co-workers[16,27,29] reported PES calculations for the major channels of this reaction and achieved good agreement between their model and experimental data on HO_2 and OH. However, this required adjustments of some well depths and barriers within the expected accuracy limits of their calculation method. Similarly, Naik[30] modified the PES at the CBS-Q level[35] to improve predictions of the C_3 mechanism. On the other hand, the earlier kinetic study on the ethyl + O_2 reaction employing the CBS-QB3 level of theory[10] to compute the PES was able to reproduce experimental results with high accuracy without any barrier adjustments, although the authors point out that this might be due to fortunate cancellation of errors. Nevertheless, the good quality of this PES was recently confirmed by Wilke et al.[36] by performing very sophisticated calculations. In general, the CBS-QB3 method has in recent years emerged as a reliable and popular tool for kinetic studies,[37,38] and, therefore, the objective of the current work is to apply this method to C_3 + O_2 reactions. Merle and co-workers[33] reported recently CBS-QB3 calculations on this system, but their focus was exclusively on the conformational distribution and decomposition pathways of alkyl peroxy radicals and not on a kinetic analysis. From comparisons to experimental data, these authors concluded that CBS-QB3 results were the most accurate among the several calculation methods tested. If we can show that the kinetic analysis of the C_3 + O_2 reaction system based on CBS-QB3 energies and molecular properties can successfully describe the major experimental observations, we could use these results to provide the database required for systematic generation of the rate rules. These rules could then confidently be applied to reactions of longer alkyl radicals with O_2, for which experimental data are not (yet) available.

Another aspect of the alkyl + O_2 chemistry is its dependence on both temperature and pressure as mentioned earlier (see Scheme 1). Previous experimental and theoretical studies on the ethyl + O_2 system[10,13,14,39] clearly demonstrate pressure effects. However, for a given temperature and pressure, unimolecular reactions of larger molecules (as a result of a higher density of states) are closer to the high-pressure limit than smaller species.[40] The same will be true for reactions of large alkyl radicals with oxygen and the question arises at what size of the alkyl radical do the rate constants for R + O_2 reactions approach the high-pressure limit. Experimental studies of OH and HO_2 production in the neopentyl + O_2[41] and cyclohexyl + O_2[42] reactions show that even for alkyl radicals containing five and six carbon atoms the high pressure limit is not fully reached for all the reaction channels under the experimental conditions employed. This conclusion holds even at pressures as high as 20.3 bar.[43] Although these observations do not necessarily mean that the kinetically most important channels are not at or close to their high pressure limits, they do indicate the need to perform a pressure-dependent analysis to investigate the influence of pressure on R + O_2 reactions, regardless of the size of the alkyl radical.

In this paper we concentrate our efforts on characterizing the kinetics of the propyl + O_2 reactions at low-temperature combustion conditions. We will demonstrate that although the PES leads to a large set of possible reaction pathways, only a few of those determine the propyl consumption and the product distributions. Similar to the previous C_2H_5 + O_2 study,[10] we find that the obtained C_3H_7 + O_2 subset based on CBS-QB3 calculations, combined with a transition state theory (TST) and Quantum Rice—Ramsperger—Kassel (QRRK) treatment, is able to reproduce experimental results quite well, at least for the considered conditions. Initial implications for the development of rate rules are also discussed. The study of addition of oxygen to γ-hydroperoxy propyl radical, which is thought to be the key to chain branching in autoignition chemistry of alkanes, will be presented as part II of this series.

II. Calculation Methods

II.1. Electronic Structure Calculations. The electronic structure calculations were carried out using the Gaussian 03 program.[44] The composite CBS-QB3 method by Peterson and co-workers[45] was selected because of its capability of predicting thermodynamic properties to "chemical accuracy", which is normally defined as within ~1 kcal/mol of experimental data. The method calculates geometries and frequencies at the B3LYP/6-311G(2d,p) level of theory. The energy is calculated at several levels of theory, including CCSD(T)/6-31+G(d′), and is then extrapolated to the complete basis set limit. All reported results for stable molecules as well as transition states were obtained for the lowest energy conformer of a given species. Normal-mode analysis was performed to verify the nature of each of these stationary points. For complicated reaction pathways, in order to confirm the correct transition state, the minimum energy paths (MEP) from the transition state to both the reactants to products were calculated using the intrinsic reaction path (IRC) method.[46,47] For several important channels, we also optimized the geometries (and calculated frequencies) at the QCISD/6-31G(d) level of theory and used those structures to calculate the CBS-QB3 energy. This was done to verify that the B3LYP geometry optimization is adequate for this reaction system. We will refer to these modified CBS-QB3 calculations as "CBS-QB3//QCISD".

II.2. Thermodynamic Property Calculations. The atomization method was employed to calculate the heats of formation of all species, and standard statistical mechanics methods were used to calculate thermodynamic properties such as entropies and heat capacities. All harmonic frequencies were scaled by a factor of 0.99 as recommended by Petersson and co-workers[45] prior to their use. Some low-frequency vibrational modes, which are better treated as internal rotations around single bonds, were replaced in the thermodynamics calculations by an explicit

evaluation of the hindered rotations. The hindrance potentials were obtained at the MP2/6-31G(d) level via relaxed surface scans with the step size of 10 degrees for dihedral angles that corresponds to the rotations. In a few cases, for which the hindrance potential calculations failed at the MP2/6-31G(d) level, those calculations were instead performed either at the B3LYP/6-31G(d) or B3LYP/6-311G(2d,p) level. The reduced moments of inertia required for the hindered rotor treatment were calculated with the approach proposed by East and Radom,[48] on the basis of the original work by Kilpatrick and Pitzer.[49] With this information at hand, the Schrödinger equations for the internal rotor could be formulated and solved numerically, and the resulting energy levels are used to calculate the partition function and the contributions to the thermodynamic functions.

II.3. Rate Constant Calculations. High-pressure rate constant calculations were carried out using canonical TST with tunneling corrections based on asymmetric Eckart potentials.[50] The high pressure rate constants for the barrierless recombination of *n*- and *i*-C_3H_7 with O_2 were not calculated in this work but derived from existing literature values.

Pressure- and temperature-dependent rate constants for the multiwell-multichannel PES were calculated based on a steady state analysis in which the energy-dependent unimolecular rate coefficients $k(E)$ were computed using the QRRK theory. The vibrational frequencies needed to calculate the density of states were extracted from an analysis of the heat capacity data calculated from the CBS-QB3 data. Collisional stabilization rate constants were calculated using the modified strong collision assumption (MSC). More details of the methodology can be found in the work of Chang et al.[51] In addition to the high-pressure rate constants, estimated Lennard−Jones collision diameters (σ_{LJ}) of 5.20 Å and well depths (ε_{LJ}) of 533 K were used for the adducts/isomers. The MSC model further requires a value for the average energy transferred per collision $\langle E_{all} \rangle$ to calculate stabilization rate constants. We used $\langle E_{all} \rangle = 250$ and 440 cal/mol for the colliders He and N_2, respectively, which are the bath gases used in the corresponding experiments. In general, the simulation results were found to be rather insensitive to the nature of the collider, at least for the conditions considered in this study.

II.4. Numerical Integration Calculations. The pressure- and temperature-dependent rate coefficients obtained from the kinetic analysis were approximated with Chebyshev polynomials over wide ranges of temperatures and pressures as proposed by Venkatesh and co-workers.[52] For constant pressure conditions, we preferably represented the rate constants in modified Arrhenius form, because this reduced the simulation times. The propyl + O_2 submechanism, consisting of all reactions together with their newly derived kinetic and thermodynamic data, was either used alone or incorporated into an existing detailed kinetic mechanism. The CHEMKIN PRO package[53] was used to predict the concentration−time profiles for comparison to the experimental results.

III. Results and Discussion

III.1. Potential Energy Surface. Although the potential energy surface for the propyl + O_2 reaction has been reported previously,[29,30,33] we reconstruct the PES with consideration of additional reaction channels using the CBS-QB3 level of theory. Our intent is to determine if CBS-QB3 theory is able to generate a PES that allows us, without adjustments, to generate rate parameters suitable to satisfactorily predict a variety of experimental data. If successful, we can use the same methodology for the generation of rate estimation rules. The PES of the C_3H_7 + O_2 at 0 K is shown in Figure 1. Even though both isomers react on the same surface, we artificially separate it in two parts, one for *n*-propyl and the other for *i*-propyl. This separation is feasible because−as we will discuss later−the reaction pathways connecting these parts are sufficiently slow that for all practical purposes both parts are, from a kinetic point of view, independent. To simplify Figure 1, dissociation channels originating from isomers **I6-I13** to form bimolecular products as well as high energy pathways are omitted.

The major features of the PES are similar to those reported in earlier studies, except that the present results are more comprehensive, for example, hydroxyl radical migration reactions are included and more product channels are considered. Since the reaction of O_2 with either propyl isomer proceeds without an energy barrier, the available energy of the initial adduct is given by that of the reactants. Several reaction pathways from the ROO• adduct proceed via barriers that are below the entrance channel. Among those are the concerted HO_2 elimination pathways from both $C_3H_7O_2$ isomers as well as isomerization to γ-hydroperoxy propyl isomers. Hydroxyl group migration reactions also have rather low barriers, and their importance cannot be ruled out a priori. Generally, it is crucial to consider this reaction class because it provides a link between the two subsets of the C_3H_7 + O_2 PES describing the reaction channels of *n*-propyl or *i*-propyl (isomer **I12).** Migration of methyl groups have not been considered due to the expected high barriers, but would also provide an interconnection between both PES parts.

In the following we discuss selected reactions proceeding on the $C_3H_7O_2$ PES in more detail.

Formation/Stabilization of Initially Formed Adduct ROO•. The strength of the formed C−O bond in alkyl peroxy radicals (or the ROO• well depth) determines the importance of the collisional stabilization channel and the temperature and pressure at which this reaction plays a role. Redissociation of ROO• is believed to be the main cause for NTC behavior.[1] Therefore, a correct value for this bond strength is an essential prerequisite for properly characterizing low-temperature oxidation.

The current results for the thermochemistry of the initially formed peroxy adducts are in good agreement with earlier calculations. Table 1 provides a comparison of the calculated C−O bond energy at 0 K for different methods. The C−O bond in *n*-$C_3H_7O_2$ is slightly weaker than in *i*-$C_3H_7O_2$. The calculated C−O bond energy in $CH_3CH_2CH_2OO$• (**I1**) is 34.8 and 35.5 kcal/mol at 0 and 298 K, respectively. These values agree well with the multistep calculations by DeSain et al.[29] (34.9 kcal/mol at 0 K), and the adjusted value used by Naik[30] (34.9 kcal/mol at 298 K). Simmie et al.[54] calculated bond energies between 34.7 and 36.6 kcal/mol at 0 K and their preferred result of 34.7 ± 0.5 kcal/mol compares favorably with our calculations. For *i*-$C_3H_7O_2$, our calculated C−O bond energy is 36.2 and 37.3 kcal/mol at 0 and 298 K, respectively. These values are also in good agreement with the value by DeSain et al. (36.8 kcal/mol at 0 K), that by Simmie et al. (36.3 ± 0.7 (preferred) at 0 K), and Naik's value (38.2 kcal/mol at 298 K). Using the CBS-QB3//QCISD method defined earlier, we obtained bond energies for both adducts that are very similar to those calculated with the regular CBS-QB3 method. This is very encouraging because it suggests that the B3LYP geometries and frequencies used in the CBS-QB3 method are of sufficient quality to obtain accurate thermodynamic data for the reactants and adducts. It is worth noting that Merle and co-workers[33] used the CBS-QB3 method to explore the ambient distribution of all possible *n*-propyl

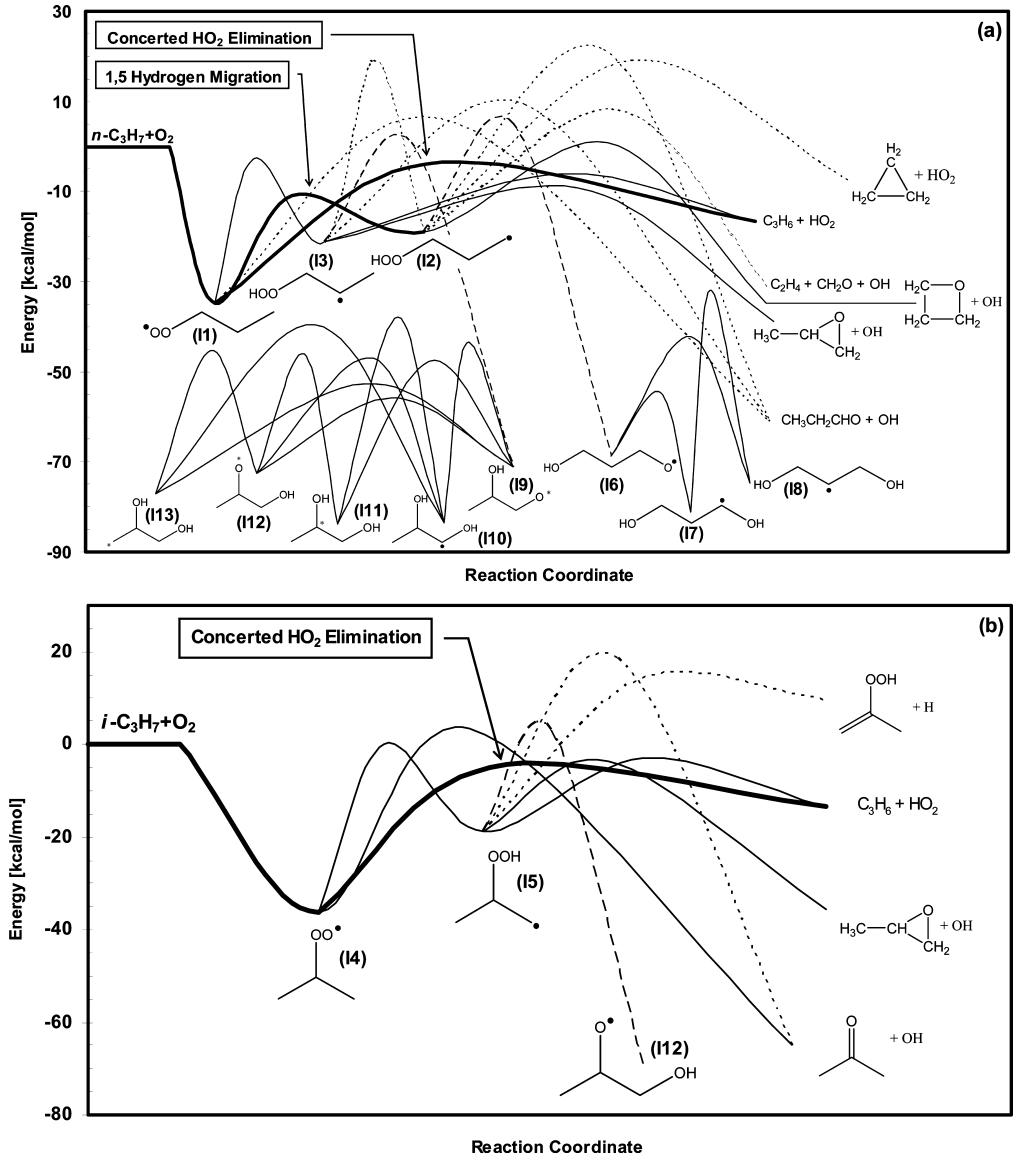

Figure 1. Potential energy diagram for the n-$C_3H_7 + O_2$ (Figure 1a) and i-$C_3H_7 + O_2$ (Figure 1b) systems at 0 K. Bimolecular product channels of isomers (**I6**)-(**I13**) are not included. Notations: $CH_3CH_2CH_2OO^{\bullet}$ (**I1**), $C^{\bullet}H_2CH_2CH_2OOH$ (**I2**), $CH_3C^{\bullet}HCH_2OOH$ (**I3**), $CH_3CH(OO^{\bullet})CH_3$ (**I4**), $C^{\bullet}H_2CH(OOH)CH_3$ (**I5**), $HOCH_2CH_2CH_2O^{\bullet}$ (**I6**), $HOCH_2CH_2C^{\bullet}HOH$ (**I7**), $HOCH_2CH^{\bullet}CH_2OH$ (**I8**), $CH_3CH(OH)CH_2O^{\bullet}$ (**I9**), $CH_3CH(OH)C^{\bullet}HOH$ (**I10**), $CH_3C^{\bullet}(OH)CH_2OH$ (**I11**), $CH_3CH(O^{\bullet})CH_2OH$ (**I12**), and $C^{\bullet}H_2CH(OH)CH_2OH$ (**I13**).

TABLE 1: Comparison of C−O Bond Energy in $C_3H_7O_2$ Radicals at 0 K. Values in Parentheses Are Calculated at 298 K (Units: kcal/mol)

species	CBS-QB3[a]	DeSain et al.[29]	Merle et al.[33]	Simmie et al.[54]	CBS-QB3//QCISD[a,b]
$CH_3CH_2CH_2OO^{\bullet}$	34.8 (35.5)	34.9	34.8 (35.8)[c]	34.7 ± 0.5 and 36.6[c]	34.6 (35.5)
$CH_3CH(OO^{\bullet})CH_3$	36.2 (37.3)	36.8		36.3 ± 0.7 and 38.7[c]	36.2 (37.3)

[a] This work. [b] See section Thermodynamic Property Calculations for details. [c] See text for details.

peroxy radical conformers. Using the reported distribution, we derived a C−O bond energy of 35.8 kcal/mol, which is only 0.3 kcal/mol higher than our value. Such an explicit consideration of all conformers requires considerably more effort and computer time than our procedure while a small improvement in the accuracy is obtained. For that reason, we chose to restrict ourselves to the lowest energy conformer but to treat the hindered rotations carefully. This approach provides a good trade-off between accuracy and CPU time demand.

Our results are also consistent with thermodynamic data reported by Knyazev and Slagle.[21] Using a mechanism that accounts for further reactions of the $ROO^{\bullet}$ adduct, they reanalyzed earlier experimental data[20] over the temperature range of 592−692 K for the reaction $CH_3C^{\bullet}HCH_3 + O_2 = CH_3CH(OO^{\bullet})CH_3$ and suggested thermodynamic values of −37.14 ± 2.23 and −37.3 cal/mol-K for ΔH°_{rxn}(298 K) and ΔS_{rxn}(298 K), respectively. These data are in excellent agreement with our CBS-QB3 values (−37.3 kcal/mol and −37.0 cal/mol-K). In addition, our calculated equilibrium constants for both $CH_3C^{\bullet}HCH_3 + O_2 = CH_3CH(OO^{\bullet})CH_3$ and $CH_3CH_2C^{\bullet}H_2 + O_2 = CH_3CH_2CH_2OO^{\bullet}$ are within a factor of 2 to those calculated by Taatjes and co-workers[27,28] in the same temperature

TABLE 2: Calculated Barrier Heights for Concerted HO_2 Elimination and Hydrogen Migration Reactions from $C_3H_7O_2$ at 0 K[a]

reactions	CBS-QB3[b]	DeSain et al.[29]	CBS-QB3//QCISD[b,c]
	Concerted HO_2 Elimination		
$CH_3CH_2CH_2OO^{\bullet} \rightarrow CH_3CH{=}CH_2 + HO_2$	30.9	29.7	31.0
	(30.3)		(30.6)
$CH_3CH(OO^{\bullet})CH_3 \rightarrow CH_3CH{=}CH_2 + HO_2$	31.2	29.8	30.8
	(30.9)		(30.6)
	Hydrogen Migration		
$CH_3CH_2CH_2OO^{\bullet} \rightarrow C^{\bullet}H_2CH_2CH_2OOH$	23.8	23.7	24.0
	(22.7)		(23.0)
$CH_3CH_2CH_2OO^{\bullet} \rightarrow CH_3C^{\bullet}HCH_2OOH$	32.1	32.3	31.7
	(31.2)		(31.0)
$CH_3CH(OO^{\bullet})CH_3 \rightarrow C^{\bullet}H_2CH(OOH)CH_3$	36.4	35.4	
	(35.8)		

[a] Values in parentheses are calculated at 298 K. (units: kcal/mol). [b] This work. [c] See section Thermodynamic Property Calculations for details.

range. Because dissociation from the $C_3H_7O_2$ adducts back to the reactants plays an important role in the reactivity of the system at moderate temperatures, the good agreement in C−O bond strengths and their related reaction thermodynamic data gives us added confidence in our simulation results.

Concerted HO_2 Elimination Reactions. This reaction class might be considered a chain-termination pathway as the HO_2 radical is relatively inert. On the $C_3H_7O_2$ PES, the adducts **I1** and **I4** form $HO_2 + C_3H_6$ with barriers of approximately 31 kcal/mol. These barriers are still below the reactant energy (−3.9 and −5.1 kcal/mol for *n*-$C_3H_7O_2$ and *i*-$C_3H_7O_2$, respectively) and therefore these channels should be important. The small difference between the barriers can in part be explained by the nature of the C−H bond that breaks during the reaction. In the case of *n*-$C_3H_7O_2$, a secondary C−H site participates in the reaction, and in addition the C−O bond in *n*-$C_3H_7O_2$ is weaker than in *i*-$C_3H_7O_2$ as discussed above (Table 1). The leaving hydrogen in the concerted HO_2 elimination reaction of *i*-$C_3H_7O_2$ stems from a primary C−H site. These differences are also reflected in the transition state structures: the HO_2 elimination reaction from *i*-$C_3H_7O_2$ proceeds through a later TS (longer C−OO and shorter OO−H bonds) than that for *n*-$C_3H_7O_2$. Table 2 provides the calculated barriers for the concerted HO_2 elimination reactions at different levels of theory. The CBS-QB3 results of this study are slightly higher than those from DeSain et al., but the difference is less than 1.5 kcal/mol. When compared with CBS-QB3//QCISD calculations, the agreement is excellent at both 0 and 298 K (less than 0.4 kcal/mol difference).

Isomerization Reactions via H Migration. These reactions play an important role in the reactivity of the propyl + O_2 system because their products, hydroperoxy alkyl radicals (Q$^{\bullet}$OOH), are believed to be the key to chain branching.[1] In addition, the ROO$^{\bullet}$ → Q$^{\bullet}$OOH isomerization is important as a step in the formation of cyclic ethers. The calculated CBS-QB3 barriers for the isomerization of propyl peroxy radicals, given in Table 2, are close to the CBS-QB3//QCISD results and to those from DeSain et al.[29] In contrast to the concerted elimination reaction, the isomerization pathways lead to a significant difference in the reactivity of *n*-$C_3H_7O_2$ compared to *i*-$C_3H_7O_2$. This is due to the 1,5-H shift reaction, which is only possible in *n*-propyl peroxy and forms $C^{\bullet}H_2CH_2CH_2OOH$. Since this reaction proceeds through a 6-membered transition state with low ring strain, its barrier height is only 22.7 kcal/mol. In comparison, the 1,4-H shift reactions in *n*- and *i*-propyl peroxy, which yield the products $CH_3C^{\bullet}HCH_2OOH$ and $C^{\bullet}H_2CH(OOH)CH_3$, respectively, have substantially higher barriers of 31.2 kcal/mol (for *n*-propyl peroxy) and 35.8 kcal/mol (for *i*-propyl peroxy) at 298 K. Again, the difference between latter barriers can be explained by the different nature of the C−OO and C−H bonds involved.

Cyclic Ether Pathways. Cyclic ethers (methyl oxirane and oxetane) formation is only possible from Q$^{\bullet}$OOH radicals, hence it requires an isomerization step. Therefore, the most likely pathway will start from $C^{\bullet}H_2CH_2CH_2OOH$. The transition state energy is only slightly below that of the initial reactants (*n*-$C_3H_7 + O_2$). Whether this reaction channel is important cannot be decided solely based on energetic grounds. Given the higher barrier for isomerization, methyl oxirane formation from $CH_3C^{\bullet}HCH_2OOH$ seems unlikely in the *n*-$C_3 + O_2$ reaction, but one needs to keep in mind that the $CH_3C^{\bullet}HCH_2OOH$ radical can also be formed via propene + HO_2, thus it will probably be an important reaction at conditions that favor high propene and HO_2 concentrations.[55]

OH Migration Reactions. In addition to hydrogen migration, hydroxyl (OH) migration reactions from Q$^{\bullet}$OOH were also included in the PES due to the weak O−O bond in the hydroperoxy group. These reactions are shown to be energetically less important than their hydrogen counterparts. For example, OH migration from **I2** to **I6**, through a 5-membered ring TS, is ∼5 kcal/mol above the reactant energy whereas the competing H migration pathway from **I2** to **I1** through a 6-membered ring transition state has the barrier of 11 kcal/mol below the reactant energy (cf. Figure 1). Similarly, the barrier for OH migration from **I3** to **I9** via a 4-membered ring TS is ∼1 kcal/mol above the reaction energy, and the competing reaction of **I3** to form methyl oxirane + OH proceeds through a barrier that is ∼10 kcal/mol lower. Hence, based on these energetic considerations, contributions from hydroxyl migration should be insignificant. A kinetic analysis confirmed this conclusion. This observation allows us to decouple the two parts of the propyl + O_2 surface, thereby simplifying the analysis of the pressure-dependence. Our conclusion is in general agreement with the work by Green et al.,[56] who have reported CBS-QB3 E_0 barriers for these two channels. Their values are even higher than ours, specifically 27.5 and 23.6 kcal/mol compared to 23.9 and 22.12 kcal/mol for **I2** → **I6** and **I3** → **I9**, leading them to conclude that the OH migration channels are not competitive, at least for the fuel ignition conditions they considered. (The differences in barriers are likely due to the different TS conformations.)

Summary. The good agreement with the literature data, together with the previous success of this method for this system[33] and the similar $C_2H_5 + O_2$ systems,[10] provides evidence that the CBS-QB3 level of theory is adequate for calculating accurate thermodynamic data for the propyl + O_2 reactions. This theory is a good compromise in terms of accuracy versus

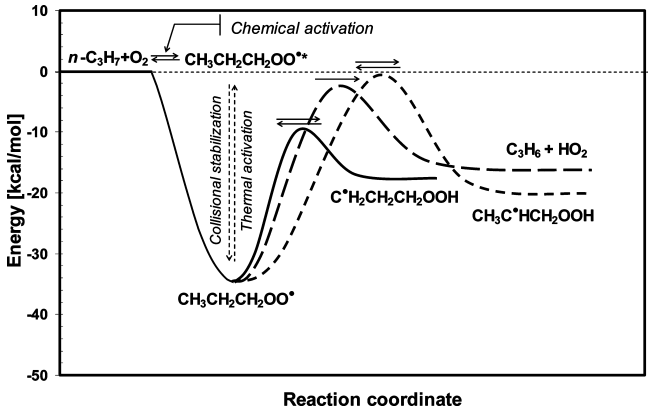

Figure 2. A portion of the potential energy diagram for the n-$C_3H_7 + O_2$ system to introduce the concepts of pressure-dependence. "*" designates an energized/activated species.

computing time requirements, especially in the context of extending this type of analysis to larger alkyl radical reactions (perhaps up to the C_6 level) with O_2. We anticipate that these results can be generalized in the form of rate rules that could then be applied reasonably confidently to $R + O_2$ reactions involving even larger alkyl radicals generated from realistic hydrocarbon fuels.

III.2. Rate Constant Calculations. ***Basic Features of Pressure Dependent Reactions.*** A complication that arises in this system is that the initially formed ROO• adduct is excited by virtue of formation of the R—O bond. This leads to a competition between unimolecular reactions of this energized adduct (e.g., isomerization and dissociation) and collisional deactivation (cf. Scheme 1). The competition means that the product branching ratios will change with temperature and pressure. These complications can be understood by considering the portion of the n-$C_3H_7 + O_2$ PES shown in Figure 2. Addition of an oxygen molecule to the n-C_3H_7 radical forms a chemically activated n-propyl peroxy radical $CH_3CH_2CH_2OO^{\bullet}$* ("*" designates an activated species). The "excess" energy of this adduct, originating from formation of the C—O bond, permits it to undergo several unimolecular reactions: (1) redissociation to the reactants, (2) formation of bimolecular products $C_3H_6 + HO_2$, (3) isomerization to $CH_3C^{\bullet}HCH_2OOH$, or (4) isomerization to $C^{\bullet}H_2CH_2CH_2OOH$. In competition with these unimolecular reactions, the energized adduct can lose energy via collisions with the bath gas to form the stabilized species, $CH_3CH_2CH_2OO^{\bullet}$. Subsequently, this stabilized species can be thermally reactivated and participate in these same unimolecular reactions; however, in general this happens on a later time scale. Because of the time-scale difference, we refer in our QRRK analysis to the products from the chemically activated adduct as "prompt" and those from the thermally activated adduct as "delayed". This physical picture is essentially the same as that used by Taatjes and co-workers.[16,27−29] They analyze the pressure-dependence of the $R + O_2$ reaction by solving the time-dependent master equation (ME). In their interpretation of their ME solutions they identify "formally direct" reaction channels in addition to the regular stabilization/thermal dissociation pathways. Both terms, "prompt" and "formally direct", therefore refer to a direct conversion of the reactants to products without the formation of a stabilized intermediate. It is worth noting at this point that the simple steady state treatment, which is used in our QRRK method, essentially retains much of the important kinetic information and compares well to the more complex time-dependent ME analysis. Since we are interested in rate constant estimation methods this is an important point, because the QRRK concept only requires high pressure rate constants as kinetic input, and thus it works well with rate estimation methods. A RRKM/ME analysis, on the other hand, is not suitable for this purpose since it requires detailed molecular information for reactants and transition states. Table 3 presents the four $R^{\bullet} + O_2$ reactions and the four ROO• reactions from the first well (**I1**) of the PES shown in Figure 2. Thermally activated reactions from the second and third stabilized isomers (**I2** and **I3**) are omitted to keep this example simple.

TABLE 3: Reactions on the Portion of the n-$C_3H_7 + O_2$ PES (cf. Figure 2)

$R^{\bullet} + O_2$ channels	
$CH_3CH_2C^{\bullet}H_2 + O_2 \rightarrow CH_3CH_2CH_2OO^{\bullet}$	(stabilization)
$CH_3CH_2C^{\bullet}H_2 + O_2 \rightarrow CH_3CH{=}CH_2 + HO_2$	(concerted elimination)
$CH_3CH_2C^{\bullet}H_2 + O_2 \rightarrow C^{\bullet}H_2CH_2CH_2OOH$	(isomerization)
$CH_3CH_2C^{\bullet}H_2 + O_2 \rightarrow CH_3C^{\bullet}HCH_2OOH$	(isomerization)
ROO• delayed channels	
$CH_3CH_2CH_2OO^{\bullet} \rightarrow CH_3CH_2C^{\bullet}H_2 + O_2$	(reverse)
$CH_3CH_2CH_2OO^{\bullet} \rightarrow CH_3CH{=}CH_2 + HO_2$	(concerted elimination)
$CH_3CH_2CH_2OO^{\bullet} \rightarrow C^{\bullet}H_2CH_2CH_2OOH$	(isomerization)
$CH_3CH_2CH_2OO^{\bullet} \rightarrow CH_3C^{\bullet}HCH_2OOH$	(isomerization)

The pressure and temperature effects for this system can be qualitatively characterized as follows. At low temperatures, the total energy in the initially formed adduct is mainly that due to bond formation, with little additional contribution from the internal energy of the reactants. As a result, the energy available for unimolecular reactions is limited, and bimolecular stabilization dominates, especially at moderate/high pressures. As the temperature increases and additional internal energy is available in the reactants, the unimolecular reactions of the energized adduct become increasingly important. For the PES shown in Figure 2, at low temperatures chemically activated $CH_3CH_2CH_2OO^{\bullet}$* will mainly be stabilized via bimolecular collisions to $CH_3CH_2CH_2OO^{\bullet}$, except for sufficiently low pressures, at which it will also form bimolecular products via unimolecular reactions. The branching ratios for the four unimolecular pathways (three product channels plus dissociation back to reactants) will depend upon both enthalpic and entropic effects. As the temperature increases, dissociation back to reactants begins to become more important since this pathway has a much higher A-factor than the various product channels. Note in Figure 2 that the reactions to form isomers are considered reversible whereas those that lead to bimolecular products are considered irreversible.

The different types of reactions naturally lead to large differences in the expected branching ratios as the pressure changes (at constant temperature). The stabilization channel of a single well system scales linearly with pressure at low pressures where bimolecular collisions are rate-limiting, whereas they become independent of pressure at high pressures. Conversely, the chemically activated unimolecular reactions of such a single well system are independent of pressure at low pressure and become inversely dependent on pressure at high pressures. The pressure-dependence becomes more complex for multiwell-multichannel systems. Thus it is essential to properly account for pressure effects in the analysis of these reactions.

High-Pressure Rate Constants. Calculation of the pressure-dependent rate coefficients using QRRK theory requires specification of the high-pressure rate coefficients for each reaction pathway. With the exception of the addition of O_2 to n-propyl and i-propyl, high-pressure rate coefficients for all the reaction pathways were calculated using unadjusted CBS-QB3 results,

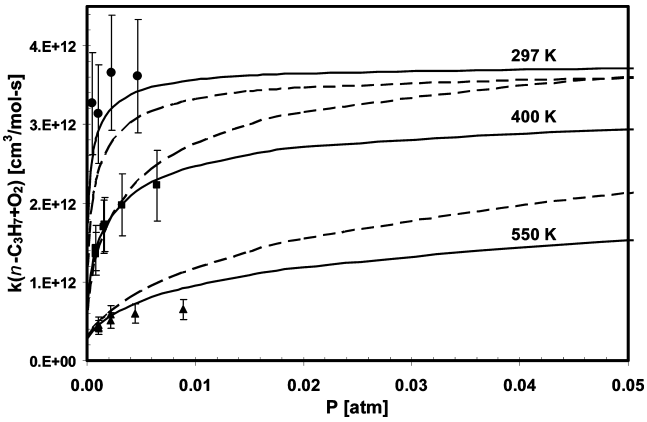

Figure 3. Comparison between experimental and predicted apparent rate coefficients for n-$C_3H_7 + O_2$ as a function of pressure and temperature. Symbols are experimental data by Slagle et al.;[19] lines are predictions with two different T^n exponents: $n = 0.52$ (dashed lines) and $n = -0.50$ (solid lines). See text for details.

following the procedure described earlier. Calculated high-pressure rate constants for all individual channels for $C_3H_7 + O_2$ systems over the temperature range 300−1500 K can be found in the accompanying Supporting Information. Addition of O_2 to n-propyl and i-propyl radicals to form ROO$^\bullet$ adducts proceeds without a barrier and special methods are required to calculate those rate coefficients. Since such calculations yield results with substantial uncertainties, we chose to assign rate coefficients for these reactions based on experiments rather than to rely on calculations. These assignments are discussed in the following paragraphs.

For the n-propyl + O_2 reaction, a value consistent with the experimental measurements of Slagle et al.[19] was selected. They used a heated tubular reactor coupled to a photoionization mass spectrometer to measure the rate coefficients. Experiments were performed at densities in the range $1.2-12 \times 10^{16}$ molecules/cm^3 and in the temperature range of 297−635 K. In these experiments, $C_6H_5C_4H_9$ and n-C_3H_7Br were used as n-propyl precursors ($C_6H_5C_4H_9 \rightarrow n$-$C_3H_7 + C_6H_5C^\bullet H_2$ and n-$C_3H_7Br \rightarrow n$-$C_3H_7 + Br$). The temporal ion signal profiles for n-C_3H_7 were fitted to a simple exponential function to obtain the pseudo first-order rate constant, k', at different O_2 concentrations. The second-order rate constant for n-$C_3H_7 + O_2$ was then obtained from the slope of plots of k' versus $[O_2]$. The data presented in Figure 3 show relatively little pressure dependence at 297 K, suggesting that the measurements are close to the high-pressure limit, thereby allowing us to fix the room-temperature value for the high-pressure rate coefficient. The next consideration is the temperature dependence. Miller and co-workers[57,58] reported a positive temperature dependence of the high-pressure rate coefficient for the reaction between ethyl radical and molecular oxygen (i.e., $k = AT^{0.52}$). Using that temperature dependence for n-propyl + O_2, the agreement between the calculated and experimental $k(T, P)$ in the falloff region is unsatisfactory, especially at high temperatures (cf. Figure 3). However, if a slightly negative temperature dependence is used instead (i.e., $k = AT^{-0.5}$), the agreement is much better. Therefore, we selected

$$k(T)_{n\text{-}C_3H_7+O_2} = 6.5 \times 10^{13} \times T^{-0.5}\ [\text{cm}^3/\text{mol}\cdot\text{s}] \quad (1)$$

as the high-pressure value for this reaction. It should be noted that our chosen negative T dependence is similar to that used by Androulakis and co-workers[34] ($T^{-0.44}$).

The next step was to select a value for the high-pressure rate coefficient for i-$C_3H_7 + O_2$. Ruiz and Bayes[22] measured rate coefficients for the reactions n-$C_3H_7 + O_2 \rightarrow$ products (Rxn I) and i-$C_3H_7 + O_2 \rightarrow$ products (Rxn II) at room temperature in a cylindrical reaction cell. Propyl radicals were monitored with photoionization mass spectrometry. The results at a few Torr total pressure suggest that both reactions are at or close to their high-pressure limits, and that the dominant products are the stabilized adducts. Ruiz and Bayes proposed high-pressure limiting values of $(3.3 \pm 0.5) \times 10^{12}$ and $(8.5 \pm 1.4) \times 10^{12}$ cm^3/mol·s for these two reactions, respectively. It is encouraging that the value derived from eq 1 at 298 K is very close to Ruiz and Bayes's value for n-$C_3H_7 + O_2$ (3.7×10^{12} vs $(3.3 \pm 0.5) \times 10^{12}$ cm^3/mol·s).

Using the measured ratio of rate coefficients at 298 K and assuming the same temperature dependence for the i-propyl reaction as for n-propyl, the high-pressure rate coefficient for $CH_3C^\bullet HCH_3 + O_2 \rightarrow CH_3CH(OO^\bullet)CH_3$ was assigned as

$$k(T)_{i\text{-}C_3H_7+O_2} = 1.63 \times 10^{14} \times T^{-0.5}\ [\text{cm}^3/\text{mol}\cdot\text{s}] \quad (2)$$

Temperature- and Pressure-Dependent Rate Constants. The calculated and assigned high-pressure rate constants were used to compute the temperature- and pressure-dependent rate constants. This QRRK analysis included all the pathways shown in Figure 1 as well as several low-barrier dissociation channels from isomers I6-I13. A complete list of the calculated rate constants for all channels over the temperature range 300−1500 K at 0.1, 1.0, and 10 atm is included in the accompanying Supporting Information. Some representative results on the effect of pressure at a temperature of 600 K for both chemically- and thermally activated reactions are presented in Figure 4. For both n-propyl and i-propyl, the dominant reaction is formation of the corresponding stabilized propyl peroxy adduct. The different pressure dependencies observed in this figure are consistent with the earlier discussion. The stabilization channels appear to be approaching the high-pressure limit near 1 atm while the rate constant for the chemically activated bimolecular product channels (Figure 4a and c) continue to decrease as pressure increases. The chemically activated concerted elimination reaction from the energized adduct is faster for i-propyl peroxy since the rate of formation of this adduct is faster. The isomerization of n-propyl peroxy to γ-hydroperoxy propyl (6-membered transition state) is an important channel, and the isomerization pathways through 5-membered transition states in n- and i-propyl peroxy are much slower due to the higher barrier. With respect to thermally activated reactions of the stabilized adducts, similar trends are seen; here the isomerization of n-propyl peroxy is fastest since this pathway has the lowest barrier. Again, all of the major pathways are near their high-pressure limiting rate constants at ~1.0 atm at this temperature. However, this is clearly not the case for minor channels such as propene + HO_2 and therefore an accurate description of the kinetics requires an analysis of the pressure effects.

The results at low pressures shown in Figure 4a illustrate some of the complexities involved in chemically activated reactions. Below ~0.3 atm the concerted elimination is faster than the isomerization even though the high-pressure rate coefficient for the isomerization is much higher. This can be explained in the following way. The isomerization reaction

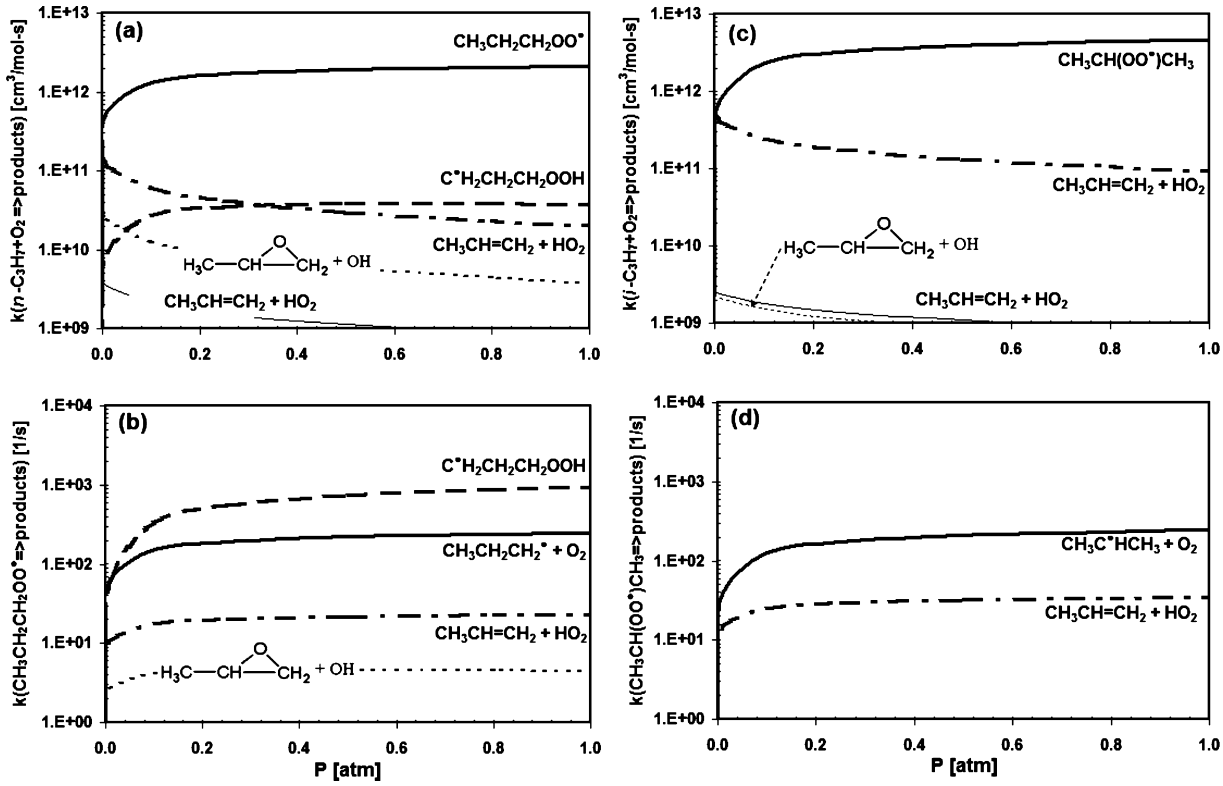

Figure 4. Rate coefficients for (a) n-$C_3H_7 + O_2 \rightarrow$ products, (b) $CH_3CH_2CH_2OO^\bullet \rightarrow$ products, (c) i-$C_3H_7 + O_2 \rightarrow$ products, and (d) $CH_3CH(OO^\bullet)CH_3 \rightarrow$ products as a function of pressure at 600 K. Only the most important reaction pathways are shown.

produces initially an excited γ-hydroperoxy propyl radical. At very low pressures, this excited species will in part convert back to the propyl peroxy radical before it is collisionally stabilized. On the other hand, the concerted elimination channel is irreversible. Once the stabilization rate increases (with increasing pressure), the isomerization pathway becomes faster than the concerted elimination, but even then the ratio of the apparent rate constants is much lower than expected on the basis of the high-pressure rate coefficients. The reason is that even after stabilization, the thermally activated reaction from the γ-hydroperoxy propyl back to propyl peroxy limits the net forward rate constant. These complexities again illustrate the necessity of properly accounting for pressure effects.

For the n-$C_3H_7 + O_2$ system in the temperature range of 300−1000 K and at pressures of larger than 0.001 atm, the most important reactions are Rxns 1−4 (cf. Table 4) whose rate constants sum up to 96% or more of the overall rate constant of n-$C_3H_7 + O_2 \rightarrow$ products. With respect to the thermally activated reactions of the stabilized propyl peroxy radical, Rxns 7−9 (Table 4) are the most important ones. Similarly, reactions Rxns 5−6 and Rxns 10−11 are the most important reactions for i-$C_3H_7 + O_2$ in the same temperature and pressure ranges. The cyclic ether channel is less important in this case. The OH migration reactions discussed earlier are even less important. Thus, in spite of the complexities of the full potential energy surface, only six chemically activated reactions and five thermally activated reactions are likely to be important for many systems of practical interest. Note that Rxns 1 and 7 are the forward and reverse of $CH_3CH_2C^\bullet H_2 + O_2 \leftrightarrow CH_3CH_2CH_2OO^\bullet$. Aside from a larger rate constant for the formation of the i-propyl peroxy radical, the major difference in the reactions of the two propyl radicals with oxygen is the availability of a low barrier isomerization pathway in the n-$C_3H_7 + O_2$ reaction, which is missing in the i-$C_3H_7 + O_2$ system.

TABLE 4: Simplified $C_3H_7 + O_2$ Submechanism

$R^\bullet + O_2$ channels	
$CH_3CH_2C^\bullet H_2 + O_2 \rightarrow CH_3CH_2CH_2OO^\bullet$	(Rxn 1)
$CH_3CH_2C^\bullet H_2 + O_2 \rightarrow C^\bullet H_2CH_2CH_2OOH$	(Rxn 2)
$CH_3CH_2C^\bullet H_2 + O_2 \rightarrow CH_3CH{=}CH_2 + HO_2$	(Rxn 3)
$CH_3CH_2C^\bullet H_2 + O_2 \rightarrow$ 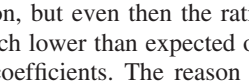	(Rxn 4)
$CH_3C^\bullet HCH_3 + O_2 \rightarrow CH_3CH(OO^\bullet)CH_3$	(Rxn 5)
$CH_3C^\bullet HCH_3 + O_2 \rightarrow CH_3CH{=}CH_2 + HO_2$	(Rxn 6)
$ROO^\bullet$ "delayed" channels	
$CH_3CH_2CH_2OO^\bullet \rightarrow CH_3CH_2C^\bullet H_2 + O_2$	(Rxn 7)
$CH_3CH_2CH_2OO^\bullet \rightarrow C^\bullet H_2CH_2CH_2OOH$	(Rxn 8)
$CH_3CH_2CH_2OO^\bullet \rightarrow CH_3CH{=}CH_2 + HO_2$	(Rxn 9)
$CH_3CH(OO^\bullet)CH_3 \rightarrow CH_3C^\bullet HCH_3 + O_2$	(Rxn 10)
$CH_3CH(OO^\bullet)CH_3 \rightarrow CH_3CH{=}CH_2 + HO_2$	(Rxn 11)

At higher temperatures, the pre-exponential term of a rate coefficient becomes increasingly more important. This is shown in Figure 5 which presents the temperature dependence of the apparent rate coefficients of the n-$C_3H_7 + O_2 \rightarrow$ product channels. The increased importance of the concerted elimination channel at higher temperature is due to its higher A-factor relative to that of the isomerization reaction, which offsets the lower activation energy of the latter reaction. The higher A-factor value for Rxn 3 can be explained by the fact that the transition state of the concerted elimination reaction (Rxn 3) ties up one

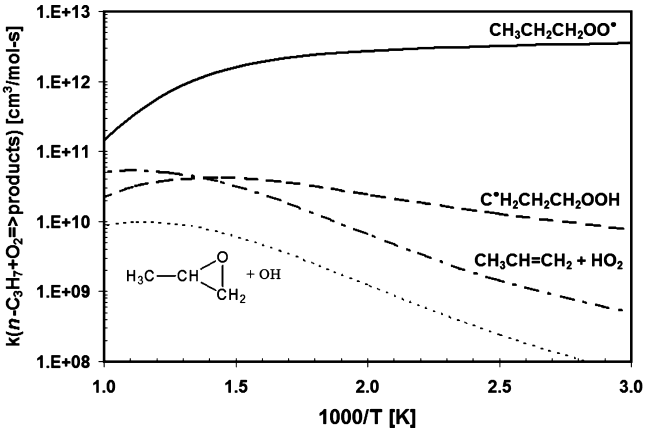

Figure 5. Rate coefficients for n-$C_3H_7 + O_2 \rightarrow$ products as a function of temperature at 1 atm. Only the most important reaction pathways are shown.

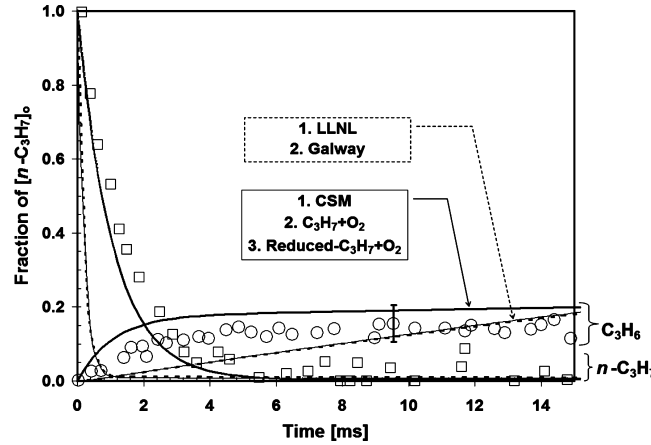

Figure 6. Time-resolved profiles of n-C_3H_7 and C_3H_6 in the study of the n-$C_3H_7 + O_2$ reaction by Slagle et al.[19] Experiments (opened circles and squares) and simulations (lines) are carried out at $T = 550$ K, [M] $= 5.94 \times 10^{16}$, $[O_2] = 6.94 \times 10^{14}$, and $[n\text{-}C_3H_7] = 5 \times 10^{11}$ molecules/cm^3. The dashed and thin solid lines are the results using the LLNL[63] and Galway[64] mechanisms, respectively. Thick solid lines: this work. See text for explanations of the three CSM models.

less hindered rotor than the transition state for the 1,5-H shift reaction (Rxn 2).

III.3. Product Prediction for Propyl + O_2 Reactions. The temperature- and pressure-dependent rate constants discussed above form the propyl + O_2 submechanism (denoted as $C_3H_7 + O_2$), which includes all the pathways shown in Figure 1 for both *n*-propyl and *i*-propyl. A subset of this submechanism, which consists of only the reactions given in Table 4, is called Reduced-$C_3H_7 + O_2$. For some of the predictions, the $C_3H_7 + O_2$ submechanism was incorporated into a larger detailed kinetic mechanism (referred to as "CSM"), which consists of a C_6 pyrolysis submechanism developed by Randolph et al.[59] and a C_3-oxidation reaction set developed by Naik et al.[60] with updated rate constants for unimolecular reactions involving C_3H_7 radicals[61] and for hydrogen abstraction at propane by HO_2.[62] The CSM mechanism is written in terms of reversible reactions whose reverse rate coefficients are calculated using the CSM thermodynamic database where group additivity was mainly used to calculate the thermodynamic properties. Because the thermodynamic properties derived from CBS-QB3 calculations for the $C_3H_7 + O_2$ subset do not exactly match those used in the CSM mechanism, these subsets were written in terms of irreversible reactions to ensure the relative thermodynamic consistency (cf. Calculation Methods) under the CBS-QB3 framework. A similar procedure was used when the Reduced-$C_3H_7 + O_2$ submechanism was incorporated into the larger mechanism ("CSM-reduced"). Predictions using either the subsets or the combined mechanisms were then compared to several different types of experiments to assess the accuracy of the $C_3H_7 + O_2$ submechanism as well as the sensitivity of the experimental data to secondary reactions.

n*-C_3H_7 *and* C_3H_6 *Profiles from n*-$C_3H_7 + O_2$ *Experiments. The first comparisons involve the time-resolved profiles of n-C_3H_7 and C_3H_6 during the n-$C_3H_7 + O_2$ experiments of Slagle et al.[19] In these experiments, $C_6H_5C_4H_9$ and n-C_3H_7Br were photolyzed to produce *n*-propyl radicals ($C_6H_5C_4H_9 \rightarrow n$-$C_3H_7 + C_6H_5C^{\bullet}H_2$ and n-$C_3H_7Br \rightarrow n$-$C_3H_7 + Br$) whose concentration was kept low to ensure that radical−radical reactions are negligible relative to *n*-propyl + O_2. The temporal ion signal profiles for n-C_3H_7 and C_3H_6 were recorded at densities in the range $1.2-12 \times 10^{16}$ molecules/cm^3 and in the temperature range of 297−635 K.

As shown in Figure 6, the CSM model is quite successful in predicting the time evolution of propylene. Since we previously used the Slagle et al. data to derive the high-pressure rate constant for the addition of O_2 to n-C_3H_7 (cf. Figure 3), it is expected that our model can characterize the n-C_3H_7 decay profile reasonably well. However, the good reproduction of the propene yield supports our kinetic analysis. Use of only the $C_3H_7 + O_2$ submechanism gives identical results, suggesting that secondary reactions are not important. Also included in Figure 6 are the predictions using the Reduced-$C_3H_7 + O_2$ submechanism, which, as anticipated, yields practically identical results.

The modeling results using mechanisms from the LLNL[63] and Galway[64] groups are also included in Figure 6. Both mechanisms yield similar predictions, which, however, are in qualitative disagreement with the experimental data. More specifically, these models, which were developed with the goal to predict NTC behavior, predict a faster decay of n-C_3H_7 and a linear increase in propylene. Since the conditions employed by Slagle et al., are far removed from ignition experiments, one would not necessarily expect that these mechanisms are able to describe the Slagle experiments, but nevertheless the comparison demonstrates that a good prediction of the propene profile is not trivial. It also demonstrates the need for comparison of model predictions to experiments over a wide range of conditions to validate a comprehensive kinetic model.

One reason for the improved performance of the CSM model under the conditions of the Slagle et al. experiments is that it includes the chemically activated reaction pathway $CH_3CH_2C^{\bullet}H_2 + O_2 \rightarrow CH_3CH{=}CH_2 + HO_2$ (Rxn 3). It allows for the "prompt" production of propylene from the reactants via the energized adduct. This reaction pathway is not included in the LLNL and Galway models. The inclusion of this chemically activated channel explains the curvature change of the C_3H_6 profile, in that much of the propylene formed comes from the chemically activated channel. It should also be noticed that the amount of C_3H_6 formed is much lower than the amount of propyl consumed. The reason for this is that the dominant reaction channel is formation of the stabilized adduct $CH_3CH_2CH_2OO^{\bullet}$. The stabilization rate constant at 0.0044 atm is about a factor 4.5 higher than that of Rxn 3. The thermally activated production of propylene is insignificant on the short time scale of this experiment.

Propylene Yields As a Function of Pressure and Temperature. Another validation opportunity is provided by a study by Kaiser and Wallington,[24] who photolyzed a mixture of

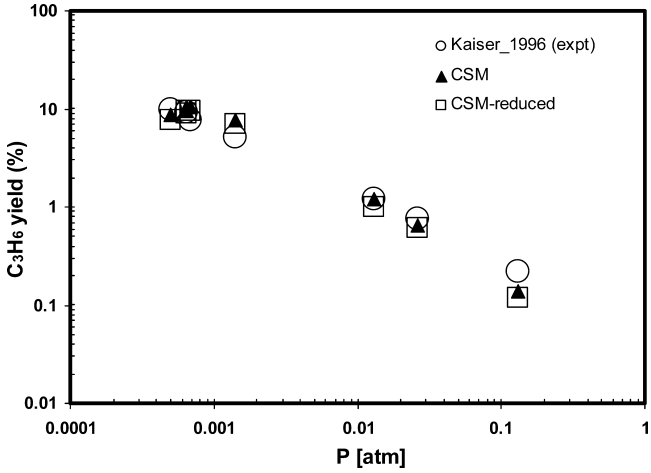

Figure 7. Plots of percentage yield of C_3H_6 vs pressure at 297 K. Experimental data are from the work of Kaiser and Wallington.[24]

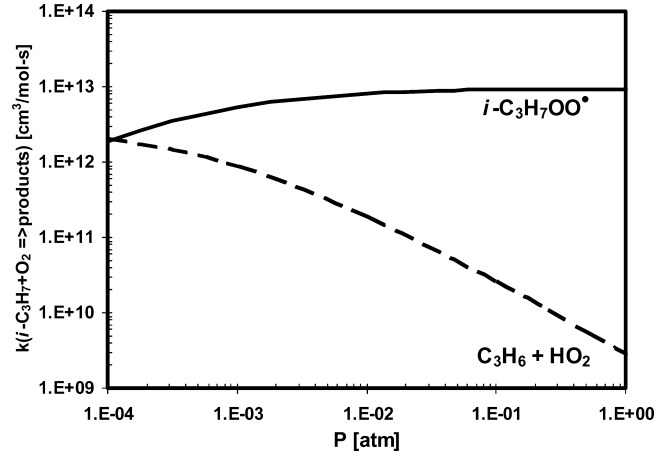

Figure 8. Rate coefficients for i-$C_3H_7 + O_2 \rightarrow$ products as a function of pressure at 298 K. Only the most important reaction pathways are shown.

propane, oxygen, and chlorine for a predetermined time and analyzed the final products by GC using flame-ionization detection. Hydrogen abstraction by photolytically produced chlorine atoms generated propyl radicals that in turn reacted with oxygen. The authors reported pressure-dependent propylene yields at 297 K.

In order to model this experiment, we added a submechanism for chlorine chemistry that is described in the accompanying Supporting Information. This submechanism is basically constructed from the work of Estupiñán and co-workers[28] with some updated reactions and rate constants that we took from the literature. The rate constant of the chlorine photolysis reaction, $Cl_2 \rightarrow 2Cl$, was adjusted to reproduce the reported propane consumption. We verified that the predictions are not very sensitive to moderate variations of this rate constant (e.g., the change of chlorine photolysis rate by a factor of 5 varies the propylene yield by less than 3%).

The CSM model with the added chlorine submechanism nicely reproduces the observed pressure dependence (cf. Figure 7). A reaction pathway analysis reveals that the reaction $CH_3C^{\bullet}HCH_3 + O_2 \rightarrow CH_3CH{=}CH_2 + HO_2$ (Rxn 6) is the main source of propylene, accounting for more than 80% of the C_3H_6 yield. The rest is formed in the chemically activated reaction of n-C_3H_7 with O_2, $CH_3CH_2C^{\bullet}H_2 + O_2 \rightarrow CH_3CH{=}CH_2 + HO_2$ (Rxn 3). The CSM-reduced model also captures the pressure-dependence of the propylene yield, but the absolute yields are slightly lower than those obtained with the full mechanism (e.g., 7.7 vs 8.8% at $P = 5 \times 10^{-4}$ Torr). The reason for the strong effect of pressure on the propylene yield is the increased dominance of the stabilization channel at higher pressures. As the pressure increases, the rate constant of the stabilization channel (i-$C_3H_7 + O_2 \rightarrow i$-$C_3H_7OO^{\bullet}$) increases to its high pressure limit, whereas that of the product channel (i-$C_3H_7 + O_2 \rightarrow C_3H_6 + HO_2$) depends inversely on the pressure (cf. Figure 8). At 298 K, this adduct is stable and subsequent thermal formation of propylene is negligible. The results shown in Figure 8 re-emphasize that, while major channels appear to be near their high-pressure limit, minor channels still depend strongly on pressure. This reinforces the need to perform detailed pressure-dependent analyses for $R + O_2$ reactions even for larger alkyl radicals, in agreement with the conclusions by Fernandes et al.[43]

In a later study, Kaiser[25] measured the effect of temperature on the formation of propylene at a constant density of $(5.5 \pm 0.5) \times 10^{18}$ molecules/cm^3. The data show a change of the

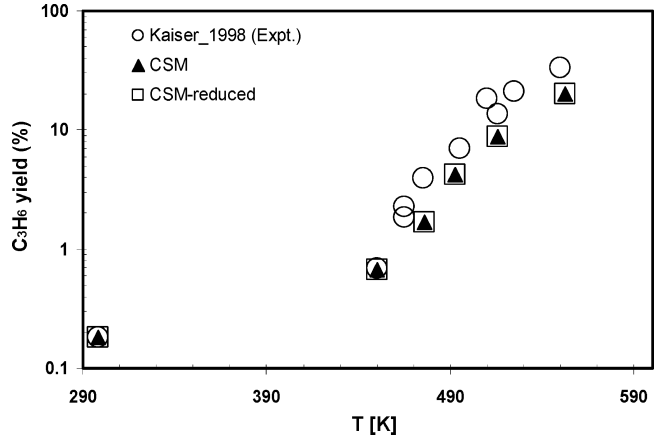

Figure 9. Percentage yield of C_3H_6 as a function of temperature at a constant density of $(5.5 \pm 0.5) \times 10^{18}$ molecules/cm^3. Initial mixture (in mole fraction) is C_3H_8 (1.05%), Cl_2 (1.80%), and O_2 (balance). Experimental data are from the work of Kaiser.[25]

propylene formation mechanism at around 450 K (cf. Figure 9). This change, which is due to the onset of thermal dissociation of the stabilized adduct, is captured by both the CSM and CSM-reduced models. The predicted absolute C_3H_6 yields at high temperatures are slightly too low, though. Such an underprediction might be due to secondary chemistry leading to C_3H_6 consumption that becomes important on the longer time scale of these experiments.

Time-Resolved HO_2 Profiles. Taatjes and co-workers[26−29] measured relative time-resolved HO_2 concentration profiles in propyl + O_2 reactions. In the chlorine-initiated experiments, alkyl radicals are formed by photolysis of either Cl_2 or CCl_3F, while propyl iodides (C_3H_7I) were photolyzed in the iodide-initiated experiments. Infrared frequency-modulation spectroscopy was used to detect HO_2.

To model the product profiles in the Cl-initiation experiments,[26] the chlorine submechanism described above was used. Figure 10 presents the comparison of the predicted and observed time-resolved profiles of HO_2, relative to the initial Cl atom concentration, at 645 K and two total densities. The simulation results from the latest model of Taatjes and co-workers[28] are also included in this figure. Both models capture the prompt production of HO_2 as well as the subsequent slower rise and ultimate decay. Of particular interest is the increase of the prompt HO_2 at the lower density, at which one would expect a larger contribution from the chemically activated pathway since

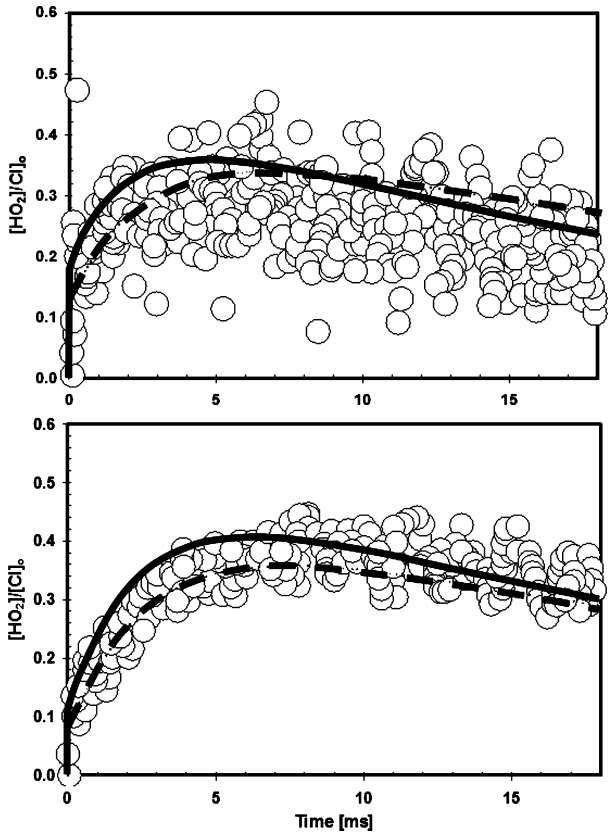

Figure 10. Comparison of the predicted (lines) and observed (open circles) time-resolved profiles, relative to the initial Cl atom concentration, for HO_2 produced in the Cl-initiated oxidation of propane at 645 K and total density of 3.65×10^{17} cm^{-3} (top panel) and 8.45×10^{17} cm^{-3} (bottom panel). Solid lines are from this study using the CSM mechanism, and dashed lines are from Taatjes and co-workers.[28] Experimental data are from the work of Taatjes and co-workers.[26,27]

there would be less collisional stabilization. This is confirmed by a rate-of-production analysis that shows that at early times (<0.08 ms) HO_2 is mainly produced by chemically activation reactions. According to the model, ~70% of HO_2 originates from i-$C_3H_7 + O_2$ and the rest is from n-$C_3H_7 + O_2$. On a longer time scale, the thermally activated production dominates. The total contribution to HO_2 production from *i*-propyl is about a factor of 2.8 higher than that from *n*-propyl radical. This observation is consistent with the previous results for propylene production by Kaiser and Wallington.[24]

Using the *n*-propyl- and *i*-propyl- iodides, Taatjes and co-workers studied the formation of HO_2 from the reactions of n-C_3H_7 and i-C_3H_7 radicals separately. We incorporated the iodine submechanism compiled from Taatjes and co-workers[28] into our kinetic model to predict the time-resolved profiles for HO_2 as well as iodine atoms. With the inclusion of iodine chemistry, the CSM mechanism can properly predict the HO_2 profiles at different conditions. Figure 11 presents a comparison of the predicted and observed time-resolved profiles for HO_2 produced in the photodissociation of *n*-propyl iodide at different temperatures and a constant total density. In general, the predictions are quite similar to both the data and the modeling results by Taatjes and co-workers. The only exception is at 703 K at which the predicted profile using our model is higher (max. 50% higher) than the observed one. However, even in this case, the shape of the profile is well predicted by the model.

With respect to the HO_2 production from the *i*-propyl + O_2 reaction, the predicted results from the CSM model again agree

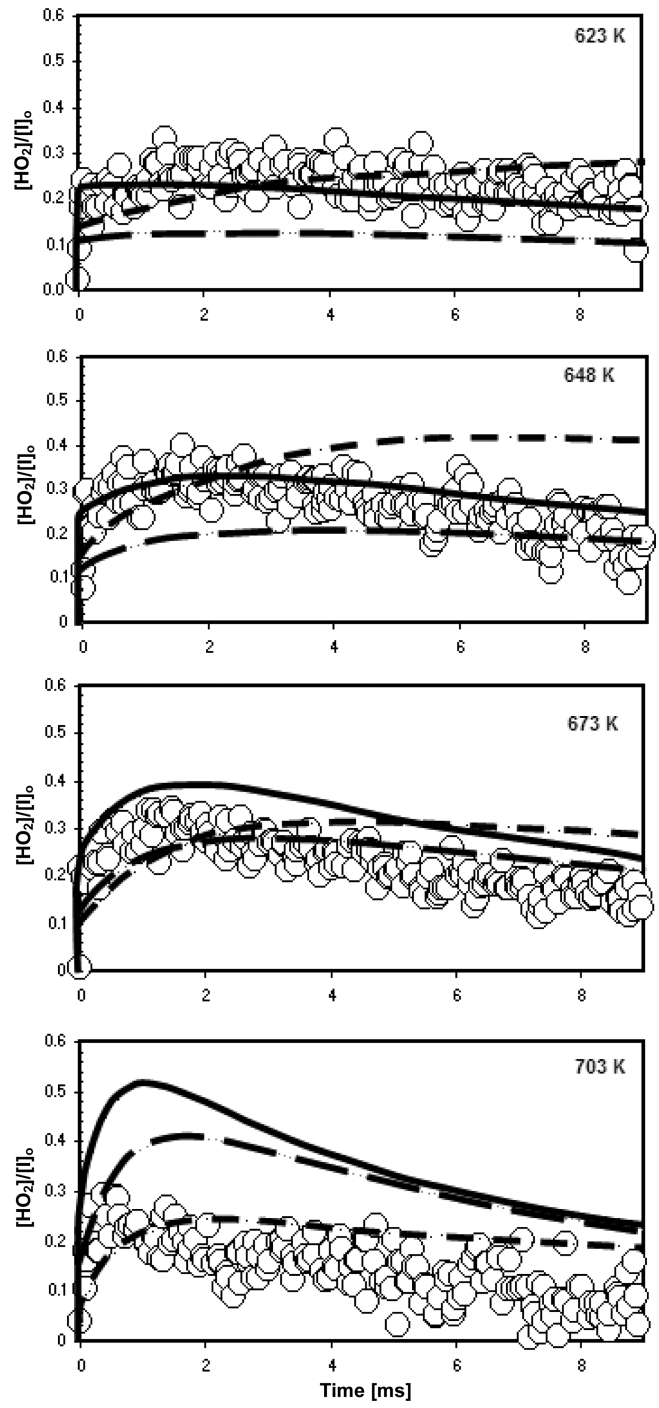

Figure 11. Comparison of the predicted (lines) and observed (open circles) time-resolved profiles, relative to the initial I atom concentration, for HO_2 produced in the photodissociation of *n*-propyl iodide at different temperatures, and a total density of 3.65×10^{17} cm^{-3}. Solid lines are from this study using the CSM mechanism; while dashed lines and experimental data are from the work of Taatjes and co-workers.[28]

well with the data at 623 and 648 K, as shown in Figure 12. However, the model begins to overpredict both prompt and overall HO_2 production at 673 K and even more so at 703 K. The predictions of Taatjes and co-workers are included for comparison. Although these are generally better for the higher temperatures, even here the agreement is not as good as at the lower temperatures.

To ascertain if a better fit could be obtained by slight adjustments of the *i*-propyl + O_2 part of the PES, we examined the impact of changes in the i-$C_3H_7OO^{\bullet}$ well-depth and the

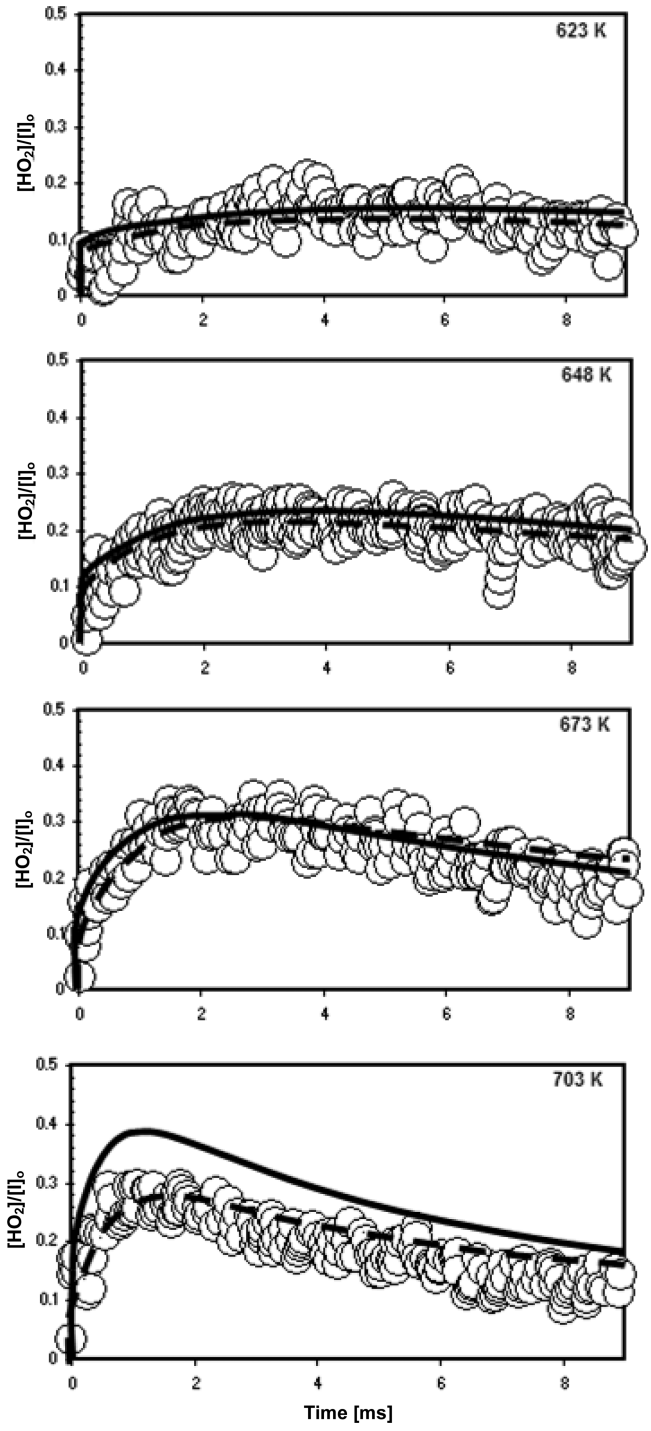

Figure 12. Comparison of the predicted (lines) and observed (open circles) time-resolved profiles, relative to the initial iodine atom concentration, for HO_2 produced in the photodissociation of *i*-propyl iodide at different temperatures and a total density of 3.65×10^{17} cm^{-3}. Solid lines are from the CSM mechanism, long dashed lines from the CSM mechanism with the barrier increase of 1 kcal/mol for HO_2 concerted elimination from *i*-$C_3H_7O_2^{\bullet}$; short dashed lines and experimental data are from the work of Taatjes and co-workers.[28]

barrier for the concerted HO_2 elimination. Although a decrease of the *i*-$C_3H_7OO^{\bullet}$ well-depth by 1 kcal/mol had little effect, an increase in the barrier height of the concerted HO_2 elimination by 1 kcal/mol significantly impacted HO_2 production, and these results are included in Figure 12. This change in the barrier improves the model prediction at high temperatures but at the expense of much poorer agreement at the lower temperatures. Thus, there is no good justification for such a change. Another modification we considered was a change in the temperature dependence of the high-pressure rate for *i*-C_3H_7 + O_2 → *i*-$C_3H_7O_2$. Not too surprisingly, this had little effect since the overall temperature range in these experiments is small.

Taatjes and workers[27,65,66] also measured the time-resolved profiles for OH. Our preliminary predictions suggest these profiles are also sensitive to other reactions (e.g., $Q^{\bullet}OOH + O_2$ and secondary reactions of OH) and thus any detailed comparisons are beyond the scope of this paper. It is noted that the production of OH via Rxn 4 (cf. Table 4) had almost no effect on any simulation results for propyl, propylene, and HO_2. Thus, we are not in a position at this time to assess the accuracy of the predicted rate expression for this channel. However, using the calculated rate constant for this reaction we find that it only plays a significant role in OH production at very low pressures (e.g., less than 0.1 atm at 600 K, cf. Figure 4a), where it dominates the other OH formation channel through the formation of γ-hydroperoxy propyl radical (formed by $CH_3CH_2CH_2OO^{\bullet}$ → $C^{\bullet}H_2CH_2CH_2OOH$) and its subsequent reactions with O_2. In other words, this reaction is likely not important under high-pressure engine conditions. Note that Wijaya et al.[67] adjusted the CBS-QB3 barrier heights for this reaction class (by changing the value of the empirical energy term in the CBS extrapolation procedure). By doing so, they obtained a higher barrier for $CH_3C^{\bullet}HCH_2OOH$ → cyclic-ether + HO_2, which leads to a substantially lower rate constant than ours at NTC conditions. Consequently, their study shows this reaction class to be even less important than our analysis suggests. Even with our larger high-pressure rate constants we observe that the cyclic ether channel is probably unimportant for all propyl + O_2 reaction systems, due to the relatively slow isomerization step required. This does not mean, that the cyclic-ether + OH channel is not important for other conditions, for example, those that favor the alkene + HO_2 reaction, as experimentally observed by Balwin et al.,[55] where the $Q^{\bullet}OOH$ radical is formed directly.

III.4. Extension toward Larger Reaction Systems. The success in characterizing many of the kinetic features of the propyl + O_2 system suggests that one can use these results as the basis to better understand the reactions of larger alkyl radicals with oxygen. Specifically, we anticipate that the types of reactions found to be important in this system will play a similar role for larger alkyl radicals. The analysis of the propyl + O_2 reaction has shown that the two most important reactions for these systems are hydrogen migration and concerted HO_2 elimination. The latter reaction is mainly responsible for the formation of propylene and HO_2. In contrast to the *n*-propyl + O_2 system, in which fast isomerization to γ-hydroperoxy propyl dominates, the addition of O_2 to *i*-propyl favors the concerted HO_2 elimination channel, thus being the main source of propylene production. Such knowledge is important in constructing rate rules for the alkyl + O_2 reaction class. The impact of the fast isomerization reaction channels leading to chain branching will be discussed in part II of this series.

Together with the previous work of Carstensen et al.[10] on C_2H_5 + O_2 at the same CBS-QB3 level, the results on the C_3H_7 + O_2 systems provide a chance to evaluate whether rate rules can be derived for important pathways for larger alkyl + O_2 reactions. Table 5 presents Arrhenius parameters for high-pressure rate constants for several isomerization reactions. (The temperature range is restricted to allow a reasonable fit; modified Arrhenius fits over a broader temperature range are provided in the Supporting Information.) As expected, we see a strong correlation between TS ring size and Arrhenius parameter

TABLE 5: High-Pressure Rate Constants for Hydrogen Migration and Concerted HO_2 Elimination Reactions (Per H Atom Basis)[a]

reaction	A	E_a	No. of restricted rotors in TS	ref
	Hydrogen Migration			
i. $CH_3CH_2OO^{\bullet} \rightarrow CH_3CHO + OH$	4.0×10^{12}	40.4	2	[b]
ii. $CH_3CH_2CH_2OO^{\bullet} \rightarrow CH_3CH_2CHO + OH$	5.0×10^{12}	39.8	2	This work
iii. $CH_3CH(OO^{\bullet})CH_3 \rightarrow CH_3C(=O)CH_3 + OH$	4.7×10^{12}	38.9	2	This work
iv. $CH_3CH_2OO^{\bullet} \rightarrow C^{\bullet}H_2CH_2OOH$	5.0×10^{11}	34.9	3	[b]
v. $CH_3CH(OO^{\bullet})CH_3 \rightarrow C^{\bullet}H_2CH(OOH)CH_3$	2.8×10^{11}	35.3	3	This work
vi. (equatorial position)	(3.6×10^{11})	(34.5)		
vii. $CH_3CH_2CH_2OO^{\bullet} \rightarrow CH_3C^{\bullet}HCH_2OOH$	3.8×10^{11}	30.6	3	This work
viii. $CH_3CH_2CH_2OO^{\bullet} \rightarrow C^{\bullet}H_2CH_2CH_2OOH$	9.3×10^{10}	23.0	4	This work
	Concerted HO_2 Elimination			
ix. $CH_3CH_2OO^{\bullet} \rightarrow C_2H_4 + HO_2$	1.1×10^{12}	31.7	2	[b]
x. $CH_3CH(OO^{\bullet})CH_3 \rightarrow C_3H_6 + HO_2$	1.7×10^{12}	31.5	2	This work
xi. $CH_3CH_2CH_2OO^{\bullet} \rightarrow C_3H_6 + HO_2$	2.0×10^{12}	30.9	2	This work

[a] All constants were computed with canonical transition state theory including corrections from Eckart tunneling and hindered rotation treatments. Rate constants are given as $k(T) = A \exp(-E_a/RT)$, valid for 550−650 K. [b] From the work of Carstensen and co-workers.[10] The units for A and E_a are 1/s and kcal/mol, respectively.

values. The decrease of the *A*-factor in reactions proceeding through larger cyclic transition states can be associated with the loss of rotors in these transition states, and the decrease in the activation energy is associated with less ring strain. For the hydrogen migration reactions that occur via a 4-membered TS (Rxns i-iii), we see very similar *A*-factors, suggesting that these could be described by a rate rule. The lower activation energy for Rxn iii is consistent with breaking a tertiary C−H versus breaking a secondary C−H bond in Rxns i and ii. Although the *A*-factors for the isomerization reactions that proceed via a 5-membered TS (Rxns iv-vi) show more variability, the trend toward a lower *A* factor and lower *E* is evident. Some of the deviations seen within this set of reactions are related to whether the methyl group is axial or equatorial (Rxns v and vi) and others are related to the transfer of primary versus secondary hydrogens (Rxns iv and vii). The trend of lower *A* and lower *E* continues for Rxn viii, which proceeds via a 6-membered TS.

The Arrhenius parameters given in Table 5 for the concerted elimination reactions are also quite similar, again suggesting the possibility of generating a rate rule that could be applicable to this reaction type in larger hydrocarbon systems. However, more data are needed to confidently assign such rate rules. Therefore, we are currently performing calculations for C_4-C_6 alkyl + O_2 reactions.

The fact that R + O_2 reactions even for larger alkyl radicals might not be at the high-pressure limit at NTC temperatures does not diminish the value of the above-discussed rate rule concept, because these data can also serve as input for a QRRK/MSC analysis. Such an analysis can even be done by an automated mechanism generation code as the work of Matheu et al.[68] demonstrated. Therefore, we are confident that these types of rate rules will in the future be of great utility in terms of assigning theoretically consistent rate constants to the reactions of larger alkyl peroxy radicals.

IV. Conclusions

We have constructed the potential energy surface for the C_3H_7 + O_2 reaction at the CBS-QB3 level of theory. Pressure- and temperature-dependent rate constants for the various channels of this system were derived using a steady-state chemical-activation analysis with high-pressure rate constants obtained from transition state theory calculations with corrections from Eckart tunneling and hindered rotation treatments. This C_3H_7 + O_2 submechanism, without adjustments of the PES, was used either directly or as part of a larger detailed kinetic mechanism to predict the temperature and pressure dependencies of the loss of propyl and the product yields of propylene and HO_2 over a wide range of temperatures, pressures, and residence times. The good overall agreement with the diverse experimental data suggests that the C_3H_7 + O_2 submechanism should be a good building block for a full propane oxidation mechanism. It was also demonstrated that only a small subset of reactions (e.g., isomerization, concerted elimination of HO_2, and stabilization) controls the oxidation kinetics, thereby considerably simplifying the mechanism. Moreover, we observed strong similarities in the rate coefficients within each of these reaction classes, suggesting the potential for developing relatively simple rate rules that can be applied to analogous reactions involving higher hydrocarbons that contain too many atoms for accurate detailed electronic structure calculation studies.

Acknowledgment. We thank Dr. W. J. Pitz and Dr. H. J. Curran for providing the LLNL and Galway mechanisms, respectively. We thank Dr. C. A. Taatjes for sending his manuscript on propyl + O_2 experiments prior to publication. The work has been supported by the Office of Naval Research (N00014-08-1-0539, program manager, Dr. David Shifler).

Supporting Information Available: (1) Tabulated values for the high-pressure rate coefficients for the C_3H_7 + O_2 system; (2) Tabulated values for the pressure-dependent apparent rate constants for the various reactions as a function of temperatures at 0.1, 1, and 10 atm; and (3) a chlorine chemistry submechanism for the chlorine-initiated experiments. This material is available free of charge via the Internet at http://pubs.acs.org.

References and Notes

(1) Walker, R. W.; Morley, C. Basic chemistry of combustion. In *Low-Temperature Combustion and Autoignition*; Pilling, M. J., Ed.; Elsevier: Amsterdam, 1997; p 1.

(2) Ranzi, E.; Faravelli, T.; Gaffuri, P.; Sogaro, A.; D'Anna, A.; Ciajolo, A. *Combust. Flame* **1997**, *108*, 24.

(3) Westbrook, C. K.; Pitz, W. J.; Herbinet, O.; Curran, H. J.; Silke, E. J. *Combust. Flame* **2009**, *156*, 181.

(4) Ranzi, E.; Faravelli, T.; Gaffuri, P.; Garavaglia, E.; Goldaniga, A. *Ind. Eng. Chem. Res.* **1997**, *36*, 3336.

(5) Pitz, W. J.; Cernansky, N. P.; Dryer, F. L.; Egolfopoulos, F. N.; Farrell, J. T.; Friend, D. G.; Pitsch, H. Development of an Experimental

Database and Chemical Kinetic Models for Surrogate Gasoline Fuels, *SAE paper 2007-01-0175*; 2007.

(6) Farrell, J. T.; Cernansky, N. P.; Dryer, F. L.; Friend, D. G.; Hergart, C. A.; Law, C. K.; McDavid, R. M.; Mueller, C. J.; Patel, A. K.; Pitsch, H. Development of an Experimental Database and Kinetic Models for Surrogate Diesel Fuels, *SAE Paper 2007-01-0201*, 2007.

(7) Colket, M.; Edwards, T.; Williams, S.; Cernansky, N. P.; Miller, D. L.; Egolfopoulos, F.; Lindstedt, P.; Seshadri, K.; Dryer, F. L.; Law, C. K.; Friend, D.; Lenhert, D. B.; Pitsch, H.; Sarofim, A.; Smooke, M.; Tsang, W. Development of an Experimental Database and Kinetic Models for Surrogate Jet Fuels, *AIAA Paper*, 2007.

(8) Curran, H. J.; Gaffuri, P.; Pitz, W. J.; Westbrook, C. K. *Combust. Flame* **1998**, *114*, 149.

(9) Rienstra-Kiracofe, J. C.; Allen, W. D.; Schaefer, H. F. III *J. Phys. Chem. A* **2000**, *104*, 9823.

(10) Carstensen, H.-H.; Naik, C. V.; Dean, A. M. *J. Phys. Chem. A* **2005**, *109*, 2264.

(11) Sheng, C.; Bozzelli, J. W.; Dean, A. M.; Chang, A. Y. *J. Phys. Chem. A* **2002**, *106*, 7276.

(12) Kaiser, E. W. *J. Phys. Chem.* **1995**, *99*, 707.

(13) Kaiser, E. W. *J. Phys. Chem. A* **2002**, *106*, 1256.

(14) Clifford, E. P.; Farrell, J. T.; DeSain, J. D.; Taatjes, C. A. *J. Phys. Chem. A* **2000**, *104*, 11549.

(15) Pilling, M. J.; Robertson, S. H.; Seakins, P. W. *Faraday Trans.* **1995**, 4179.

(16) Taatjes, C. A. *J. Phys. Chem. A* **2006**, *110*, 4299.

(17) Baker, R. R.; Baldwin, R. R.; Walker, R. W. *Trans. Faraday Soc.* **1970**, *66*, 3016.

(18) Baldwin, R. R.; Walker, R. W.; Yorke, D. A. *J. Chem. Soc., Faraday Trans. 1* **1973**, *69*, 826.

(19) Slagle, I. R.; Park, J.-Y.; Gutman, D. *Proc. Combust. Inst.* **1984**, *20*, 733.

(20) Slagle, I. R.; Ratajczak, E.; Heaven, M. C.; Gutman, D.; Wagner, A. F. *J. Am. Chem. Soc.* **1985**, *107*, 1838.

(21) Knyazev, V. D.; Slagle, I. R. *J. Phys. Chem. A* **1998**, *102*, 1770.

(22) Ruiz, R. P.; Bayes, K. D. *J. Phys. Chem.* **1984**, *88*, 2592.

(23) Gulati, S. K.; Walker, R. W. *J. Chem. Soc. Trans. 2* **1988**, *84*, 401.

(24) Kaiser, E. W.; Wallington, T. J. *J. Phys. Chem.* **1996**, *100*, 18770.

(25) Kaiser, E. W. *J. Phys. Chem. A* **1998**, *102*, 5903.

(26) DeSain, J. D.; Clifford, E. P.; Taatjes, C. A. *J. Phys. Chem. A* **2001**, *105*, 3205.

(27) DeSain, J. D.; Klippenstein, S. J.; Miller, J. A.; Taatjes, C. A. *J. Phys. Chem. A* **2003**, *107*, 4415.

(28) Estupiñán, E. G.; Klippenstein, S. J.; Taatjes, C. A. *J. Phys. Chem. B* **2005**, *109*, 8374.

(29) DeSain, J. D.; Taatjes, C. A.; Miller, J. A.; Klippenstein, S. J.; Hahn, D. K. *Faraday Discuss.* **2001**, *119*, 101.

(30) Naik, C. V. Modeling the Low to Intermediate Temperature Oxidation and Pyrolysis of Hydrocarbons, Ph.D. thesis, Colorado School of Mines, 2004.

(31) Chan, W.-T.; Hamilton, I. P.; Pritchard, H. O. *J. Chem. Soc., Faraday Trans.* **1998**, *94*, 2303.

(32) Chan, W.-T.; Pritchard, H. O.; Hamilton, I. P. *Phys. Chem. Chem. Phys.* **1999**, *1*, 3715.

(33) Merle, J. K.; Hayes, C. J.; Zalyubovsky, S. J.; Glover, B. G.; Miller, T. A.; Hadad, C. M. *J. Phys. Chem. A* **2005**, *109*, 3637.

(34) Androulakis, I. P.; Grenda, J. M.; Barckholtz, T. A.; Bozzelli, J. W. *AIChE J.* **2006**, *52*, 3246.

(35) Bozzelli, J. W. New Jersey Institute of Technology, private communication, 2004.

(36) Wilke, J. J.; Allen, W. D.; Schaefer, H. F. *J. Chem. Phys.* **2008**, *128*, 074308.

(37) Vandeputte, A. G.; Sabbe, M. K.; Reyniers, M.-F.; Speybroeck, V. V.; Waroquier, M.; Marin, G. B. *J. Phys. Chem. A* **2007**, *111*, 11771.

(38) Carstensen, H.-H.; Dean, A. M. *J. Phys. Chem. A* **2009**, *113*, 367.

(39) Slagle, I. R.; Feng, Q.; Gutman, D. *J. Phys. Chem.* **1984**, *88*, 3648.

(40) Wong, B. M.; Matheu, D. M.; Green, W. H. *J. Phys. Chem. A* **2003**, *107*, 6206.

(41) DeSain, J. D.; Klippenstein, S. J.; Taatjes, C. A. *Phys. Chem. Chem. Phys.* **2003**, *5*, 1584.

(42) Knepp, A. M.; Meloni, G.; Jusinski, L. E.; Taatjes, C. A.; Cavallotti, C.; Klippenstein, S. J. *Phys. Chem. Chem. Phys.* **2007**, *9*, 4315.

(43) Fernandes, R. X.; Zádor, J.; Jusinski, L. E.; Miller, J. A.; Taatjes, C. A. *Phys. Chem. Chem. Phys.* **2009**, *11*, 1320.

(44) Frisch, M. J.; Trucks, G. W.; Schlegel, H. B.; Scuseria, G. E.; Robb, M. A.; Cheeseman, J. R.; Montgomery, J. A.; Jr., T. V.; Kudin, K. N.; Burant, J. C.; Millam, J. M.; Iyengar, S. S.; Tomasi, J.; Barone, V.; Mennucci, B.; Cossi, M.; Scalmani, G.; Rega, N.; Petersson, G. A.; Nakatsuji, H.; Hada, M.; Ehara, M.; Toyota, K.; Fukuda, R.; Hasegawa, J.; Ishida, M.; Nakajima, T.; Honda, Y.; Kitao, O.; Nakai, H.; Klene, M.; Li, X.; Knox, J. E.; Hratchian, H. P.; Cross, J. B.; Adamo, C.; Jaramillo, J.; Gomperts, R.; Stratmann, R. E.; Yazyev, O.; Austin, A. J.; Cammi, R.; Pomelli, C.; Ochterski, J. W.; Ayala, P. Y.; Morokuma, K.; Voth, G. A.; Salvador, P.; Dannenberg, J. J.; Zakrzewski, V. G.; Dapprich, S.; Daniels, A. D.; Strain, M. C.; Farkas, O.; Malick, D. K.; Rabuck, A. D.; Raghavachari, K.; Foresman, J. B.; Ortiz, J. V.; Cui, Q.; Baboul, A. G.; Clifford, S.; Cioslowski, J.; Stefanov, B. B.; Liu, G.; Liashenko, A.; Piskorz, P.; Komaromi, I.; Martin, R. L.; Fox, D. J.; Keith, T.; Al-Laham, M. A.; Peng, C. Y.; Nanayakkara, A.; Challacombe, M.; Gill, P. M. W.; Johnson, B.; Chen, W.; Wong, M. W.; Gonzalez, C.; Pople, J. A. *Gaussian 03, Revision A.1*; Gaussian, Inc.: Pittsburgh, PA, 2003.

(45) Montgomery, J. A., Jr.; Frisch, M. J.; Ochterski, J. W.; Petersson, G. A. *J. Chem. Phys.* **1999**, *110*, 2822.

(46) Gonzalez, C.; Schlegel, H. B. *J. Chem. Phys.* **1989**, *90*, 2154.

(47) Gonzalez, C.; Schlegel, H. B. *J. Phys. Chem.* **1990**, *94*, 5523.

(48) East, A. L. L.; Radom, L. *J. Chem. Phys.* **1997**, *106*, 6655.

(49) Kilpatrick, J. E.; Pitzer, K. S. *J. Chem. Phys.* **1949**, *28*, 1064.

(50) Eckart, C. *Phys. Rev.* **1930**, *35*, 13031.

(51) Chang, A. Y.; Bozzelli, J. W.; Dean, A. M. *Z. Phys. Chem.* **2000**, *214*, 1533.

(52) Venkatesh, P. K.; Chang, A. Y.; Dean, A. M.; Cohen, M. H.; , R. W.; Carr, J. *AIChE J.* **1997**, *43*, 1331.

(53) CHEMKIN-PRO; Reaction Design: San Diego, 2008.

(54) Simmie, J. M.; Black, G.; Curran, H. J.; Hinde, J. P. *J. Phys. Chem. A* **2008**, *112*, 5010.

(55) Baldwin, R. R.; Dean, C. E.; Walker, R. W. *J. Chem. Soc., Faraday Trans.2* **1986**, *82*, 1445.

(56) Green, W. H.; Wijaya, C. D.; Yelvington, P. E.; Sumathi, R. *Mol. Phys.* **2004**, *102*, 371.

(57) Miller, J. A.; Klippenstein, S. J. *Int. J. Chem. Kinet.* **2001**, *33*, 654.

(58) Miller, J. A.; Klippenstein, S. J.; Robertson, S. H. *Proc. Combust. Inst.* **2000**, *28*, 1479.

(59) Randolph, K. L.; Dean, A. M. *Phys. Chem. Chem. Phys.* **2007**, *9*, 4245.

(60) Naik, C. V.; Dean, A. M. *Combust. Flame* **2006**, *145*, 16.

(61) TST rate with Eckart tunneling and hindered rotation treatmens at CBS-QB3//QCISD level.

(62) Aguilera-Iparraguirre, J.; Curran, H. J.; Klopper, W.; Simmie, J. M. *J. Phys. Chem. A* **2008**, *112*, 7047.

(63) Pitz, W. J. Lawrence Livermore National Laboratories, private communication, 2009.

(64) Gallagher, S. M.; Curran, H. J.; Metcalfe, W. K.; Healy, D.; Simmie, J. M.; Bourque, G. *Combust. Flame* **2008**, *153*, 316.

(65) DeSain, J. D.; Klippenstein, S. J.; Miller, J. A.; Taatjes, C. A. *J. Phys. Chem. A* **2004**, *108*, 7127.

(66) Taatjes, C. A. Sandia National Laboratories, private communication, 2010.

(67) Wijaya, C. D.; Sumathi, R.; Green, W. H. *J. Phys. Chem. A* **2003**, *107*, 4908.

(68) Matheu, D. M.; Dean, A. M.; Grenda, J. M.; Green, W. H. *J. Phys. Chem. A* **2003**, *107*, 8552.

JP1017218